

# Engineering the surface of LiCoO<sub>2</sub> electrodes using atomic layer deposition for stable high-voltage lithium ion batteries

Jin Xie<sup>1</sup>, Jie Zhao<sup>1</sup>, Yayuan Liu<sup>1</sup>, Haotian Wang<sup>2</sup>, Chong Liu<sup>1</sup>, Tong Wu<sup>1</sup>, Po-Chun Hsu<sup>1</sup>, Dingchang Lin<sup>1</sup>, Yang Jin<sup>1</sup>, and Yi Cui<sup>1,3</sup> (✉)

<sup>1</sup> Department of Materials Science and Engineering, Stanford University, Stanford, CA 94305, USA

<sup>2</sup> Department of Applied Physics, Stanford University, Stanford, CA 94305, USA

<sup>3</sup> Stanford Institute for Materials and Energy Sciences, SLAC National Accelerator Laboratory, Menlo Park, CA 94025, USA

**Received:** 25 January 2017

**Revised:** 7 March 2017

**Accepted:** 12 March 2017

© Tsinghua University Press  
and Springer-Verlag Berlin  
Heidelberg 2017

## KEYWORDS

Lithium ion batteries,  
lithium cobalt oxide,  
atomic layer deposition

## ABSTRACT

Developing advanced technologies to stabilize positive electrodes of lithium ion batteries under high-voltage operation is becoming increasingly important, owing to the potential to achieve substantially enhanced energy density for applications such as portable electronics and electrical vehicles. Here, we deposited chemically inert and ionically conductive LiAlO<sub>2</sub> interfacial layers on LiCoO<sub>2</sub> electrodes using the atomic layer deposition technique. During prolonged cycling at high-voltage, the LiAlO<sub>2</sub> coating not only prevented interfacial reactions between the LiCoO<sub>2</sub> electrode and electrolyte, as confirmed by electrochemical impedance spectroscopy and Raman characterizations, but also allowed lithium ions to freely diffuse into LiCoO<sub>2</sub> without sacrificing the power density. As a result, a capacity value close to 200 mA·h·g<sup>-1</sup> was achieved for the LiCoO<sub>2</sub> electrodes with commercial level loading densities, cycled at the cut-off potential of 4.6 V vs. Li<sup>+</sup>/Li for 50 stable cycles; this represents a 40% capacity gain, compared with the values obtained for commercial samples cycled at the cut-off potential of 4.2 V vs. Li<sup>+</sup>/Li.

## 1 Introduction

Ever since the commercialization of lithium ion batteries, LiCoO<sub>2</sub> has been widely used as a positive electrode material [1, 2]. The combination of its relatively high discharge plateau and high tapped density makes LiCoO<sub>2</sub> an ideal material to provide high specific

energy density and volumetric energy density, both of which are important criteria for energy storage solutions. Even today, the majority of mobile electronics are powered by LiCoO<sub>2</sub>-based lithium ion batteries. However, emerging applications such as the electrification of the transportation system, where the stability, safety, and efficiency of batteries are of great

Address correspondence to yicui@stanford.edu

concern, demand superior capabilities as well as provide great opportunities for lithium ion batteries [3–6].

The potential application of LiCoO<sub>2</sub>-based cathodes in electrical vehicles has been hindered by the poor stability of LiCoO<sub>2</sub> when cycled with a high cut-off potential or at elevated temperatures. In spite of a high theoretical capacity of 272 mA·h·g<sup>-1</sup>, only ~0.5 Li<sup>+</sup> per LiCoO<sub>2</sub> (~137 mA·h·g<sup>-1</sup>) is utilized in the lithiation/delithiation process to prevent severe side reactions, which typically occur at an accelerated rate when LiCoO<sub>2</sub> cathodes are cycled beyond 4.2 V vs. Li<sup>+</sup>/Li [2, 5, 6]. The side reactions could lead to fast capacity decay and, more importantly, safety hazards. To solve the above-mentioned dilemma between high capacity and long stability, a variety of surface modification methods have been proposed to protect LiCoO<sub>2</sub> from degradation [7–11]. The majority of the surface coating processes are based on solution phase methods to coat metal oxides—such as ZrO<sub>2</sub>, Al<sub>2</sub>O<sub>3</sub>, and SiO<sub>2</sub>—on individual LiCoO<sub>2</sub> particles [7–9, 12, 13]. Although the direct coating process on particles has been shown to be easy-to-handle and cost-effective, the coating layers may break and expose fresh LiCoO<sub>2</sub> surfaces during harsh slurry mixing and electrode calendaring processes. In addition, the power density is sacrificed as the low ionic and electronic conductivities of the coating materials may create barriers in between LiCoO<sub>2</sub> particles. Therefore, a more effective strategy to coat metal oxides on the entire LiCoO<sub>2</sub> electrode has been demonstrated by several groups by using atomic layer deposition (ALD) [10, 11, 14, 15]. While the electrode stability improved after coating, the power density was inevitably compromised, as most metal oxides prepared by ALD are poor lithium ion conductors. To solve this problem, an effective coating with both excellent chemical stability and ionic conductivity is needed.

Here, we explore ALD of LiAlO<sub>2</sub> thin films directly on LiCoO<sub>2</sub> electrodes with a commercial level of loading to improve their stability without sacrificing power density or energy density. While effective LiAlO<sub>2</sub> coating on LiCoO<sub>2</sub> particles by using solution phase synthesis has been reported by Cao et al. [16], the strategy of direct and uniform ALD coating at the electrode scale provides two important advantages. First, electrical conductivity in between individual

particles is not compromised, as the coating is conducted directly on the electrode level. The nature of the ALD technique ensures that the coating occurs on the surface, generating a uniform thin film covering the entire electrode while maintaining the interconnectivity of the LiCoO<sub>2</sub> particles. The sequence of slurry coating and calendaring, followed by the final ALD coating, also minimizes the possibility of film cracking during processing. Second, as ALD processes are flexible and integrable, different ALD chemistries can be combined to design more complex thin films [17–20]. Another dilemma of using ALD to coat battery electrodes arises from the compromise between electrochemical stability and rate capability. Typical ALDs follow an island nucleation model, with subsequent linear growth; often times, the resulting metal-oxide films are poor lithium ion conductors. Therefore, on the one hand, thick and uniform coating, which would effectively protect LiCoO<sub>2</sub> from degrading, limits the power performance of coated electrodes. Conversely, thin coatings enable LiCoO<sub>2</sub> to show good power densities even after thin-film coating, but have limited stability enhancement as the coating is non-uniform (island nucleation), allowing not only lithium ions to pass through, but also side reactions to occur. In this work, by doping Li<sub>2</sub>O into Al<sub>2</sub>O<sub>3</sub>, the resulting LiAlO<sub>2</sub> coating layer allowed Li ions to pass through and, at the same time, prevented side reactions between the electrolyte and LiCoO<sub>2</sub> surface. Owing to the presence of a LiAlO<sub>2</sub> thin-film interfacial layer on the surface of the LiCoO<sub>2</sub> electrode, the increase in cell impedance upon cycling could be significantly suppressed, and the formation of the Co<sub>3</sub>O<sub>4</sub> phase on the surface of the LiCoO<sub>2</sub> electrodes during overcharging was prevented. As a result, improved cycling stability with a wide electrochemical window and at an elevated temperature was achieved.

## 2 Results and discussion

While thin-film coating may improve the stability of electrode materials [7–11], it also raises two critical challenges: retaining power density and energy density after coating. As shown in Fig. 1(a), we propose coating the LiCoO<sub>2</sub> electrode with LiAlO<sub>2</sub> directly by using ALD to simultaneously preserve the electron transport

pathways and lithium ion transport pathways. First,  $\text{LiAlO}_2$  thin films were directly deposited on  $\text{LiCoO}_2$  electrodes instead of  $\text{LiCoO}_2$  powders. The merit of this electrode fabrication sequence is to prevent electrical polarization in between individual  $\text{LiCoO}_2$  particles. In addition, it minimizes the possibility of film cracking during slurry mixing and electrode calendaring processes. Second,  $\text{LiAlO}_2$  is a solid electrolyte with lithium ion conductivity depending on various factors including Li/Al ratio, film orientation, thickness, and crystallinity [17, 21–23]. Aaltonen et al. first demonstrated that  $\text{LiAlO}_2$  films could be obtained via ALD by alternating  $\text{Li}_2\text{O}$  and  $\text{Al}_2\text{O}_3$  ALD sub-cycles during the  $\text{LiAlO}_2$  ALD process [22], and the lithium ion conductivity of  $\text{LiAlO}_2$  improved significantly, compared with that of pure  $\text{Al}_2\text{O}_3$  films [17, 23].

In this study,  $\text{LiAlO}_2$  thin films were deposited by alternating  $\text{Li}_2\text{O}$  (lithium isopropoxide and water) and  $\text{Al}_2\text{O}_3$  (trimethylaluminum and water) ALD sub-cycles, using an exposure mode to achieve uniform coverage on  $\text{LiCoO}_2$  electrodes with high surface area (Fig. 1(a)). For characterization purposes,  $\text{LiAlO}_2$  films were first deposited on ball-milled  $\text{LiCoO}_2$  powders for ease of transmission electron microscopy (TEM) observation.

In Fig. 1(b), 20 cycles of ALD  $\text{LiAlO}_2$  (10 super-cycles; one super-cycle consists of one  $\text{Li}_2\text{O}$  sub-cycle and one  $\text{Al}_2\text{O}_3$  sub-cycle) were performed. A uniform thin-film coating with thickness close to 2 nm was obtained. When the deposition thickness was increased further after performing 200 ALD cycles, the  $\text{LiCoO}_2$  core and  $\text{LiAlO}_2$  shell structures could be clearly mapped using energy-dispersive spectroscopy (EDX; Fig. 1(c)). To check elemental compositions and calculate film thicknesses quantitatively, inductively coupled plasma mass spectrometry (ICP-MS) was performed, and the results are summarized in Figs. 1(d) and 1(e).  $\text{LiAlO}_2$  films were deposited on silicon wafers, and then dissolved by  $\text{HNO}_3$  solution to avoid complications from Li in  $\text{LiCoO}_2$ . The areal loading density of Li and Al increased linearly with the number of ALD cycles, and the Li to Al mole ratio in the film was close to 1.5. The growth rate of  $\text{Al}_2\text{O}_3$  in the  $\text{Al}_2\text{O}_3$  sub-cycles of the  $\text{LiAlO}_2$  ALD process was found to be close to that observed for the pure  $\text{Al}_2\text{O}_3$  ALD process (Fig. S2 in the Electronic Supplementary Material (ESM)). In addition to ICP-MS, X-ray photoelectron spectroscopy (XPS) was also performed to check the elemental composition of the as-deposited films on the surface.

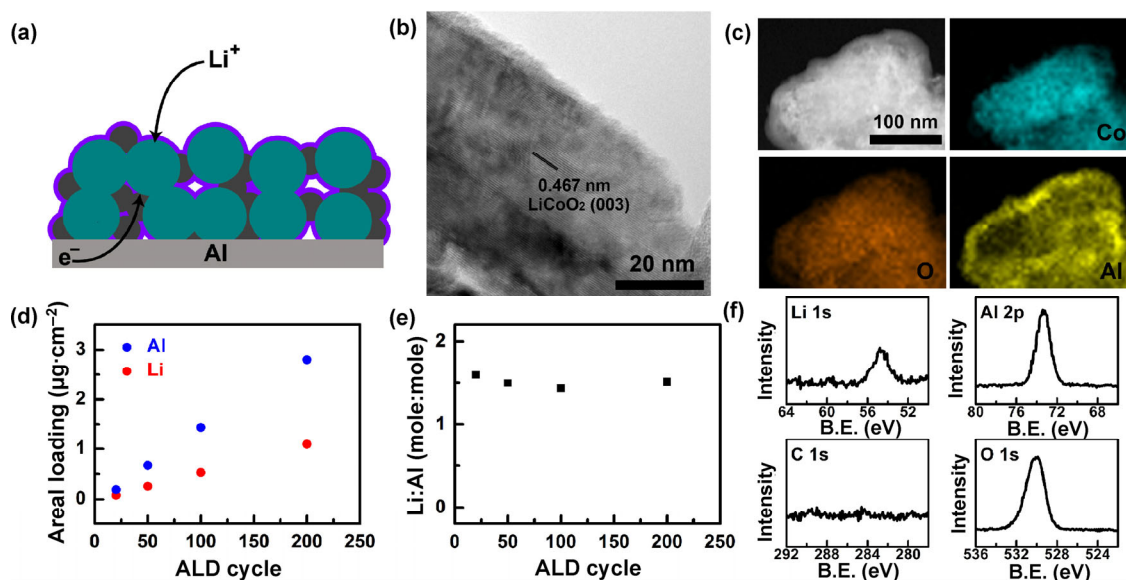


**Figure 1** (a) Scheme of  $\text{LiAlO}_2$  coating (purple) on  $\text{LiCoO}_2$  electrode (dark cyan for  $\text{LiCoO}_2$  particles and dark grey for conductive carbon) by atomic layer deposition (ALD); (b) transmission electron microscopy characterization of a 20-cycle-ALD  $\text{LiAlO}_2$  coated  $\text{LiCoO}_2$  particle; (c) energy-dispersive spectroscopy mapping of a 200-cycle-ALD  $\text{LiAlO}_2$  coated  $\text{LiCoO}_2$  particle; (d) Li and Al areal loading density in ALD  $\text{LiAlO}_2$  films grown on Si wafers, as detected by inductively coupled plasma mass spectrometry (ICP-MS); (e) Li to Al molar ratio in ALD  $\text{LiAlO}_2$  films grown on Si wafers, as detected by ICP-MS; (f) X-ray photoelectron spectroscopy characterizations of 200-cycle-ALD  $\text{LiAlO}_2$  film grown on Si wafer.

After performing a mild sputtering treatment for 6 s to remove surface-absorbed carbon impurities, no carbon residue from ALD precursors was detected (Fig. 1(f)), indicating high film quality.

The  $\text{LiAlO}_2$  coating was performed on  $\text{LiCoO}_2$  electrodes made from industrial  $\text{LiCoO}_2$  powders. For all tests, unless specified, commercial  $\text{LiCoO}_2$  powder purchased from MTI was dried and mixed with Super C65 and polyimide (PI) with a mass ratio of 90:5:5 to make cathodes with an average loading of  $15 \text{ mg}_{\text{LiCoO}_2} \cdot \text{cm}^{-2}$ . Commercial poly(vinylidene fluoride) (PVDF) binder was replaced with PI, owing to the low melting point of PVDF, which is below the ALD operation temperature. The rate performances of electrodes with and without coating layers were tested using a typical electrochemical window ranging from 2.75 to 4.20 V vs.  $\text{Li}^+/\text{Li}$  for  $\text{LiCoO}_2$  (Fig. 2(a)). At a low rate ( $10 \text{ mA} \cdot \text{g}^{-1}$ ), the average discharge capacity of a pristine cathode in the first five cycles approached  $142.3 \text{ mA} \cdot \text{h} \cdot \text{g}^{-1}$ . In comparison, cathodes with 20-cycle-ALD  $\text{LiAlO}_2$  coating showed almost identical discharge capacity ( $140.1 \text{ mA} \cdot \text{h} \cdot \text{g}^{-1}$ ) and similar charge/discharge profiles (Fig. 2(b)). The capacities of  $\text{LiAlO}_2$  coated

samples were close to those of the pristine  $\text{LiCoO}_2$  samples at all rates (10, 20, and  $50 \text{ mA} \cdot \text{g}^{-1}$ ), except for a slight difference at the highest rate of  $100 \text{ mA} \cdot \text{g}^{-1}$  (Fig. 2(c)). Conversely, 20-cycle-ALD  $\text{Al}_2\text{O}_3$  (without lithium doping) coated  $\text{LiCoO}_2$  exhibited significantly lower capacity than pristine  $\text{LiCoO}_2$  at all rates (10, 20, 50, and  $100 \text{ mA} \cdot \text{g}^{-1}$ ). Even at the lowest rate of  $10 \text{ mA} \cdot \text{g}^{-1}$ , the average discharge capacities of the 20-cycle-ALD  $\text{Al}_2\text{O}_3$  coated cathodes in the first five cycles were lower than  $100 \text{ mA} \cdot \text{h} \cdot \text{g}^{-1}$ , presumably owing to the uniform coverage of the  $\text{Al}_2\text{O}_3$  films deposited by 20 cycles of ALD and the poor lithium ion conductivity of  $\text{Al}_2\text{O}_3$ .

The challenge of high energy density can be overcome by minimizing the loading of inactive coating materials and extending the electrochemical window of  $\text{LiCoO}_2$ .  $\text{LiAlO}_2$  or  $\text{Al}_2\text{O}_3$  coating films obtained by up to 50 cycles of ALD were less than 1% of the active  $\text{LiCoO}_2$  weight. The uniformity of the ALD coating allows using the minimum amount of inactive materials to coat high surface area electrodes, which has been a challenge in solution phase synthesis or solid-state synthesis. More importantly, it is always

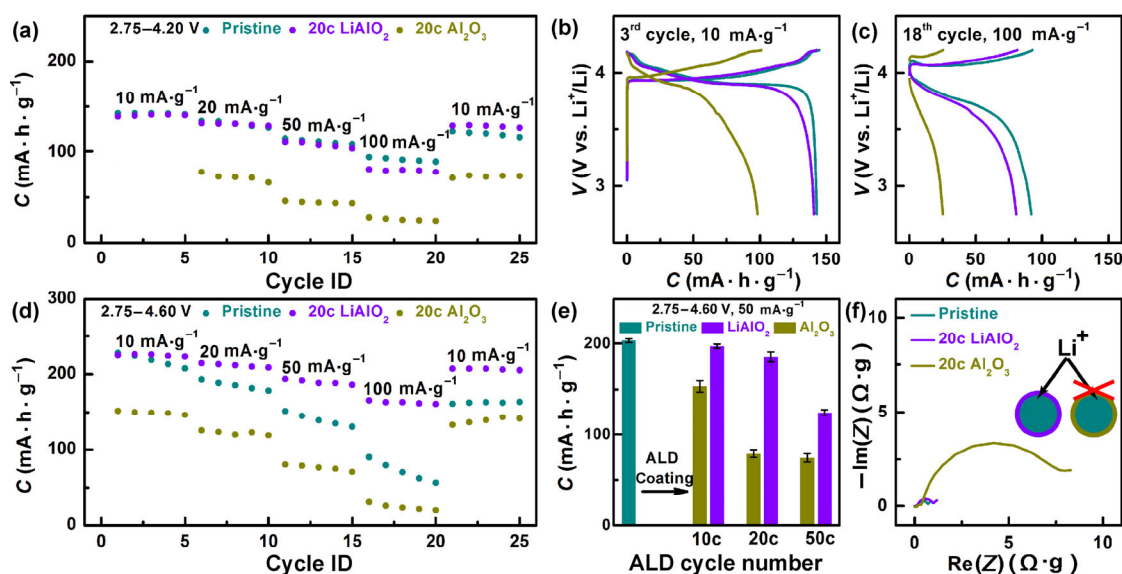


**Figure 2** Electrochemical measurements. (a) Rate performance of pristine, 20-cycle atomic layer deposition (ALD)  $\text{LiAlO}_2$  coated and 20-cycle-ALD  $\text{Al}_2\text{O}_3$  coated  $\text{LiCoO}_2$  electrodes tested with an electrochemical window of 2.75–4.20 V vs.  $\text{Li}^+/\text{Li}$ ; (b) and (c) detailed voltage vs. capacity profiles of pristine, 20-cycle-ALD  $\text{LiAlO}_2$  coated, and 20-cycle-ALD  $\text{Al}_2\text{O}_3$  coated  $\text{LiCoO}_2$  electrodes tested in Fig. 2(a) at the 3<sup>rd</sup> cycle ( $10 \text{ mA} \cdot \text{g}^{-1}$ ) and 18<sup>th</sup> cycle ( $100 \text{ mA} \cdot \text{g}^{-1}$ ); (d) rate performance of pristine, 20-cycle-ALD  $\text{LiAlO}_2$  coated, and 20-cycle-ALD  $\text{Al}_2\text{O}_3$  coated  $\text{LiCoO}_2$  electrodes tested with an electrochemical window of 2.75–4.60 V vs.  $\text{Li}^+/\text{Li}$ ; (e) comparison of 1<sup>st</sup> cycle discharge capacities of pristine,  $\text{LiAlO}_2$  coated, and  $\text{Al}_2\text{O}_3$  coated  $\text{LiCoO}_2$  electrodes with an electrochemical window of 2.75–4.60 V vs.  $\text{Li}^+/\text{Li}$  at  $50 \text{ mA} \cdot \text{g}^{-1}$ ; (f) electrochemical impedance spectroscopy characterizations of pristine, 20-cycle-ALD  $\text{LiAlO}_2$  coated, and 20-cycle-ALD  $\text{Al}_2\text{O}_3$  coated  $\text{LiCoO}_2$  electrodes after the 1<sup>st</sup> cycle.

of practical interest to extend the electrochemical windows during cycling, in order to extract more lithium ions out of  $\text{LiCoO}_2$  for even greater energy density. However, the pristine  $\text{LiCoO}_2$  cathode showed severe capacity degradation within a few cycles (Fig. 2(d)) when the electrochemical window was aggressively expanded to 2.75–4.60 V vs.  $\text{Li}^+/\text{Li}$ . In comparison, both  $\text{LiAlO}_2$  coated and  $\text{Al}_2\text{O}_3$  coated samples showed decent capacity retention, while the  $\text{LiAlO}_2$  coated samples were able to deliver a significantly higher specific capacity than the  $\text{Al}_2\text{O}_3$  coated samples, owing to the ability to conduct lithium ions in  $\text{LiAlO}_2$ . As the pristine cathodes degraded rapidly within a few cycles, the statistical results of the first-cycle specific capacities of cathodes with and without thin-film coating are here presented to illustrate the correlation between film thickness/composition and achievable capacity with a wider electrochemical window (Fig. 2(e)). In the 1<sup>st</sup> cycle, at the relatively fast cycling rate of  $50 \text{ mA}\cdot\text{g}^{-1}$ , the  $\text{Al}_2\text{O}_3$  coating of the  $\text{LiCoO}_2$  electrodes provided low specific capacities. After only 20 cycles of ALD  $\text{Al}_2\text{O}_3$  coating, the specific capacity dropped to  $79.0 \pm 4.1 \text{ mA}\cdot\text{h}\cdot\text{g}^{-1}$  from  $203.3 \pm 2.3 \text{ mA}\cdot\text{h}\cdot\text{g}^{-1}$  of the pristine electrodes. Electrochemical impedance spectroscopy (EIS) was also conducted on the samples after the 1<sup>st</sup> charge cycle, showing a significantly increased impedance after 20 cycles of ALD  $\text{Al}_2\text{O}_3$  coating. In the case of the ALD  $\text{LiAlO}_2$  coated electrodes, lithium ions could diffuse into  $\text{LiCoO}_2$  through the  $\text{LiAlO}_2$  thin film, thus exhibiting a considerably higher initial capacity (i.e.,  $185.5 \pm 5.4 \text{ mA}\cdot\text{h}\cdot\text{g}^{-1}$  with 20-cycle-ALD  $\text{LiAlO}_2$  vs.  $79.0 \pm 4.1 \text{ mA}\cdot\text{h}\cdot\text{g}^{-1}$  with 20-cycle-ALD  $\text{Al}_2\text{O}_3$ ). When compared with the pristine  $\text{LiCoO}_2$  electrode, the  $\text{LiAlO}_2$  coated electrodes exhibited indeed a slight decrease in initial capacity and increase in impedance; thus, further efforts to develop lithium ion conductive coating films with higher conductivity by using ALD are needed.

As  $\text{Al}_2\text{O}_3$  is not a good lithium ion conductor, the conduction of lithium ions through a protective  $\text{Al}_2\text{O}_3$  film has to go through pinholes. Such defects are inevitable when considering: (1) The island nucleation model of atomic-layer-deposited  $\text{Al}_2\text{O}_3$ , which grows forming discrete particles instead of a continuous thin film in the early stage of the ALD process [24]; (2) film cracking in post-growth operations including

electrode handling, coin-cell fabrication, and  $\text{LiCoO}_2$  particle cracking during cycling [25]. While these defects allow lithium ions to conduct through at a discounted rate, compared with what observed in pristine samples, they also lead to similar electrode degradation as in pristine samples. For example, although the  $\text{LiCoO}_2$  electrode with 10-cycle-ALD  $\text{Al}_2\text{O}_3$  coating showed appreciable capacity in the first few cycles, its capacity decayed at a rate only slightly slower than that of the pristine  $\text{LiCoO}_2$  electrode (Fig. 3(a)). Conversely, while the stability could be improved by increasing the  $\text{Al}_2\text{O}_3$  coating thickness after performing 20 ALD cycles, the overall capacity dropped.

The dilemma mentioned above can be solved by using a  $\text{LiAlO}_2$  coating, as shown by the tests conducted with the 2.75–4.60 V electrochemical window at the cycling rate of  $50 \text{ mA}\cdot\text{g}^{-1}$  (Fig. 3(a)). EIS was conducted under the same test conditions after different numbers of battery cycles for the  $\text{LiAlO}_2$  coated  $\text{LiCoO}_2$  electrode (Fig. 3(b)). The impedance spectra remained almost unchanged after 50 cycles, which explained the good capacity retention of the  $\text{LiAlO}_2$  coated  $\text{LiCoO}_2$  electrode cycled with high voltage cutoffs. The detailed impedance spectra of the  $\text{LiAlO}_2$  coated  $\text{LiCoO}_2$  electrode were also compared with those of the pristine  $\text{LiCoO}_2$  electrode side by side after 1, 5, 10, 25, and 50 battery cycles (Figs. 3(c)–3(g)). At the end of the 1<sup>st</sup> charge cycle, the impedance spectra of both samples with and without coating comprised two semicircles and a straight line angled close to  $45^\circ$ . The small semicircle at high frequency was related to the solid electrolyte interface, while the one at medium frequency corresponded to the charge transfer at the cathode/electrolyte interface [26]. The  $45^\circ$  inclined line at low frequency was due to the Warburg impedance, which can be attributed to the diffusion of lithium ions within the  $\text{LiCoO}_2$  cathode [27]. Upon battery cycling, the semicircle at medium frequency increased significantly for the pristine  $\text{LiCoO}_2$  electrode, indicating the slowdown of charge transport across the cathode/electrolyte interface. Although the initial charge transfer resistance was slightly higher for  $\text{LiAlO}_2$  thin film coated samples (Fig. 3(c)), the coating layer helped suppress the fast impedance increase seen in the following cycles for pristine  $\text{LiCoO}_2$  electrodes (Figs. 3(d)–3(g)).

The stabilities of pristine and  $\text{LiAlO}_2$  coated

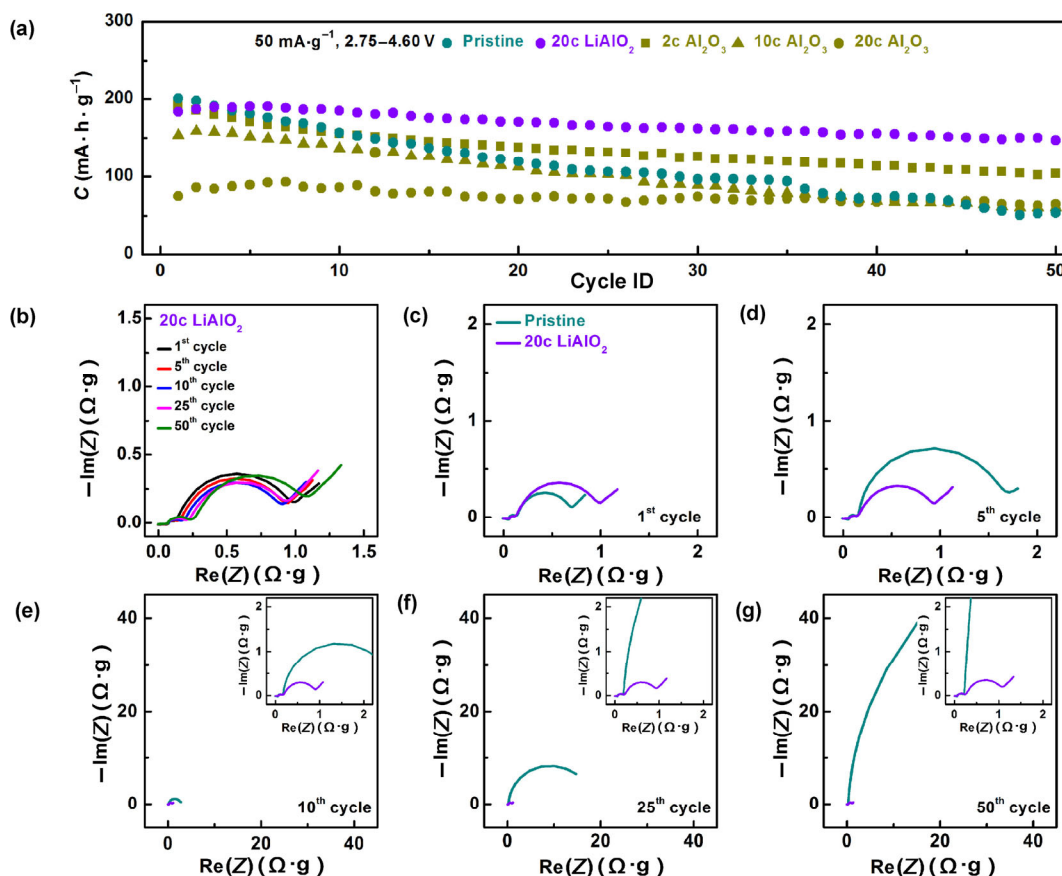


**Figure 3** Electrochemical measurements. (a) Cycle performance of pristine, 20-cycle-ALD LiAlO<sub>2</sub> coated, and 2-, 10-, 20-cycle-ALD Al<sub>2</sub>O<sub>3</sub> coated LiCoO<sub>2</sub> electrodes; (b) summary of electrochemical impedance spectroscopy characterizations of 20-cycle-ALD LiAlO<sub>2</sub> coated LiCoO<sub>2</sub> electrode at the end of the 1<sup>st</sup>, 5<sup>th</sup>, 10<sup>th</sup>, 25<sup>th</sup>, and 50<sup>th</sup> cycle; (c)–(g) comparison of impedance spectra of pristine LiCoO<sub>2</sub> electrodes and 20-cycle-ALD LiAlO<sub>2</sub> coated LiCoO<sub>2</sub> electrodes at the end of the 1<sup>st</sup>, 5<sup>th</sup>, 10<sup>th</sup>, 25<sup>th</sup>, and 50<sup>th</sup> cycle. The cycling tests were performed with a 2.75–4.60 V vs. Li<sup>+</sup>/Li electrochemical window at room temperature and current density of 50 mA·g<sup>-1</sup>.

LiCoO<sub>2</sub> electrodes were tested under different cycling conditions and at various temperatures. At the lower cycling rate of 20 mA·h·g<sup>-1</sup>, the capacity of the pristine LiCoO<sub>2</sub> electrode quickly dropped from 218.8 to 117.9 mA·h·g<sup>-1</sup> in 50 cycles, when cycled with the same 2.75–4.60 V vs. Li<sup>+</sup>/Li electrochemical window. In contrast, the specific capacity of the LiAlO<sub>2</sub>-protected cathode only slightly dropped from 198.7 to 172.2 mA·h·g<sup>-1</sup> in 50 cycles (Fig. 4(a)). In addition to the stability towards a wide electrochemical window, the stability of LiCoO<sub>2</sub> electrodes when cycled at elevated temperature is a practical requirement for applications such as electrical vehicles. For instance, the capacity of the pristine LiCoO<sub>2</sub> electrode faded at an accelerated rate when tested at 50 °C (only 28.7 mA·h·g<sup>-1</sup> left at the 50<sup>th</sup> cycle, Fig. 4(b)). The high-temperature stability of LiCoO<sub>2</sub> could be improved

via LiAlO<sub>2</sub> ALD coating. After 50 battery cycles, it still possessed a discharge capacity of 143.0 mA·h·g<sup>-1</sup>, which was almost four times higher than that of pristine LiCoO<sub>2</sub> samples after 50 cycles.

Many different mechanisms have been proposed to explain the instability of LiCoO<sub>2</sub> cycled with a wide electrochemical window; these include, but are not limited to, electrolyte oxidation by delithiated LiCoO<sub>2</sub> [28, 29], mechanical breakdown induced by phase transition [12, 13, 25], and cobalt dissolution [30]. Next, we present our efforts in EIS, X-ray diffraction (XRD), and Raman spectroscopy to identify one possible failure mechanism for the LiCoO<sub>2</sub> electrode when cycled with a wide electrochemical window, and understand how the LiAlO<sub>2</sub> thin-film protection prevents the electrode failure. Our hypothesis is that Li<sub>1-x</sub>CoO<sub>2</sub> becomes highly unstable when deeply

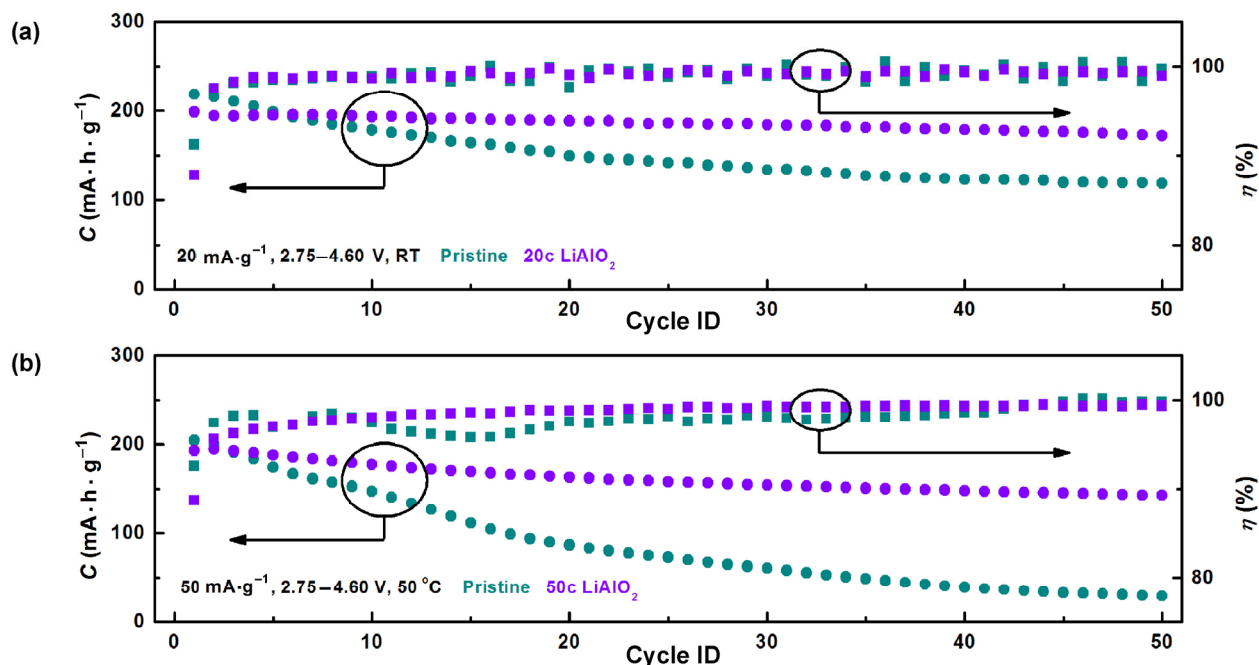


**Figure 4** Electrochemical measurements. (a) Cycle performance of pristine and 20-cycle atomic layer deposition (ALD) LiAlO<sub>2</sub> coated LiCoO<sub>2</sub> electrodes with a current density of 20 mA·g<sup>-1</sup> at room temperature; (b) cycle performance of pristine and 50-cycle-ALD LiAlO<sub>2</sub> coated LiCoO<sub>2</sub> electrodes with a current density of 50 mA·g<sup>-1</sup> at elevated temperature (50 °C). Squares indicate Coulombic efficiencies while circles indicate discharge capacities. All cycling tests were performed within a 2.75–4.60 V vs. Li<sup>+</sup>/Li electrochemical window.

delithiated at high applied potentials. It could either self-decompose through disproportionation reactions or oxidize the electrolyte. Both pathways release oxygen from the unstable Li<sub>1-x</sub>CoO<sub>2</sub> lattice to form Co<sub>3</sub>O<sub>4</sub> as one of the side products. The accumulation of side products increases the impedance of the battery and leads to a decreased capacity. As discussed earlier, the EIS measurements (Figs. 3(b)–3(g)) suggested that the decrease in specific capacity was directly related to the increase in cell impedance at the cathode/electrolyte interface. To further validate this assumption, pristine LiCoO<sub>2</sub>/Li cells after 50 cycles of battery cycling were disassembled, and the impedance spectrum was recorded. Then, all cell components, except the cycled LiCoO<sub>2</sub> electrode itself, were replaced by fresh ones. As shown in Fig. 5(b), the largest impedance in a cycled LiCoO<sub>2</sub>/Li cell was clearly associated with the cathode. Changing other cell components could not reduce the already large impedance or restore the battery capacity.

Through detailed characterization of the electrodes, the origin of the high measured impedance at the interface after cycling was identified. After 50 cycles

of aggressive lithiation and delithiation, the LiCoO<sub>2</sub> electrode was subjected to XRD examination. In the case of the cycled electrode, all the peaks identified in the XRD pattern belonged to the LiCoO<sub>2</sub> phase, and no other significant peaks appeared (Fig. 5(c)), suggesting that minimum impurities with well-defined crystalline grain sizes were formed. To detect changes at the interface, we then conducted *ex situ* Raman mapping on pristine and LiAlO<sub>2</sub> coated LiCoO<sub>2</sub> electrodes after battery cycling. In Fig. 5(d), the spectrum of a LiAlO<sub>2</sub> coated LiCoO<sub>2</sub> electrode after 50 battery cycles, mapped using a 532 nm laser, is shown (more details in the ESM). The Raman spectra showed two sets of characteristics peaks for LiCoO<sub>2</sub> (Co–O stretching (A<sub>1g</sub>) at 594 cm<sup>-1</sup> and O–Co–O bending (E<sub>g</sub>) at 483 cm<sup>-1</sup>) and carbon (D-band (A<sub>1g</sub>) at ~1,355 cm<sup>-1</sup> and G-band (E<sub>2g2</sub>) at ~1,590 cm<sup>-1</sup>). The peak positions were in good agreement with the standard values reported in Ref. [31] and our measurements from a pristine LiCoO<sub>2</sub> electrode prior to cycling (Fig. S7 in the ESM). The intensity of the LiCoO<sub>2</sub> E<sub>g</sub> peak was then integrated and mapped, and its shape agreed well with the optical images of

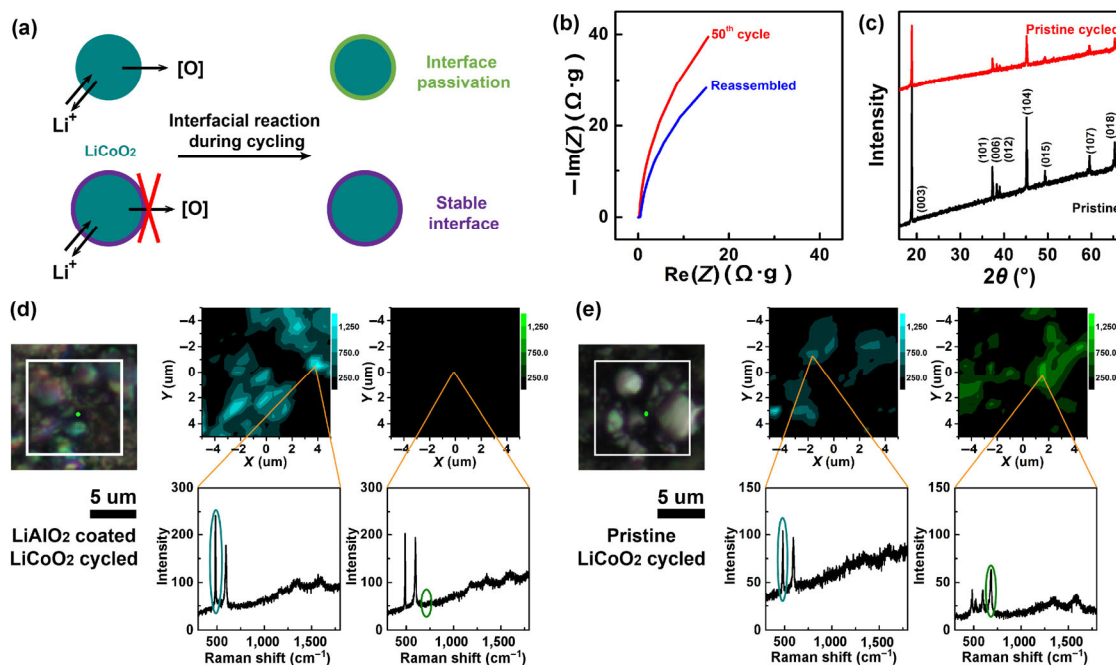


**Figure 5** (a) Schematic illustration of possible fading mechanism of LiCoO<sub>2</sub> electrode under high voltage cycling; cyan circles indicate LiCoO<sub>2</sub> particles, green circle indicates the surface passivation layer, and violet circle indicates the stable LiCoO<sub>2</sub> interfacial layer; (b) electrochemical impedance spectroscopy characterizations of pristine LiCoO<sub>2</sub>/Li coin cell after 50 cycles (red trace) and reassembled coin cell using the cycled pristine LiCoO<sub>2</sub> (blue trace); (c) X-ray diffraction patterns of pristine LiCoO<sub>2</sub> electrode prior to cycling (black trace) and pristine LiCoO<sub>2</sub> electrode after 50 battery cycles (red trace); (d) Raman mapping of LiAlO<sub>2</sub> coated LiCoO<sub>2</sub> electrode surface after 50 battery cycles; (e) Raman mapping of pristine LiCoO<sub>2</sub> electrode surface after 50 battery cycles. For the Raman mapping, the white-highlighted square area in the optical image was mapped.

the LiCoO<sub>2</sub> electrode. When mapping pristine LiCoO<sub>2</sub> after cycling (Fig. 5(e)), the most striking difference was the emergence of Co<sub>3</sub>O<sub>4</sub> peaks. Although characteristic LiCoO<sub>2</sub> and carbon peaks still existed in some regions, new peaks at 520 and 683 cm<sup>-1</sup> emerged in some other regions. These two peaks, which correspond to one of the three active F<sub>2g</sub> modes and one A<sub>1g</sub> mode of Co<sub>3</sub>O<sub>4</sub>, were in good agreement with those observed in reported Co<sub>3</sub>O<sub>4</sub> Raman spectra [32] and standard tested Co<sub>3</sub>O<sub>4</sub> Raman spectra (Fig. S7 in the ESM). The intensity of the Co<sub>3</sub>O<sub>4</sub> A<sub>1g</sub> peak was integrated and mapped. The results showed that the formed Co<sub>3</sub>O<sub>4</sub> phase partially overlapped with optical images of LiCoO<sub>2</sub>. Upon analysis of the information gathered, the following hypothesis for the degradation of the LiCoO<sub>2</sub> electrode, when cycled with a wide electrochemical window, was formulated. The fading of the LiCoO<sub>2</sub>/Li cell starts at the interface between LiCoO<sub>2</sub> and electrolyte. When deeply delithiated, LiCoO<sub>2</sub> becomes unstable, and could potentially lose oxygen to form Co<sub>3</sub>O<sub>4</sub>. As shown in the supplementary

information, Co<sub>3</sub>O<sub>4</sub> electrodes, even made of Co<sub>3</sub>O<sub>4</sub> nanoparticles with a size of 10–30 nm, were unable to host lithium ions in the tested 2.75–4.60 V vs. Li<sup>+</sup>/Li electrochemical window (Fig. S5 in the ESM). The formation of the Co<sub>3</sub>O<sub>4</sub> phase has been observed by other groups as well [33, 34]. For ALD LiAlO<sub>2</sub> protected cathodes, such phase transition from LiCoO<sub>2</sub> to Co<sub>3</sub>O<sub>4</sub> at the interface was not observed. The lack of phase transition was attributed to the chemical stability of the LiAlO<sub>2</sub> film, which prevented interfacial reactions between LiCoO<sub>2</sub> and electrolyte.

### 3 Conclusions

In this work, we demonstrated that, by using ALD to form a LiAlO<sub>2</sub> thin-film coating directly on the LiCoO<sub>2</sub> electrode, improved stability over a wide electrochemical window and at elevated temperature can be achieved without sacrificing energy density or power density. The detailed capacity fading mechanism of the LiCoO<sub>2</sub> electrode under aggressive cycling

conditions was also investigated. The results suggested that the formation of an inactive interfacial layer could lead to increased cell impedance and significant polarization. By encapsulating  $\text{LiCoO}_2$ , the  $\text{LiAlO}_2$  thin-film coating shows promising potential for improving battery stability for high-voltage battery operation.

## 4 Experimental

### 4.1 Materials synthesis and preparation

$\text{LiCoO}_2$  (MTI Inc., see Fig. S3 in the ESM for more details), Super C65 (Imerys), and PI (DuPont) were dried under vacuum for 24 h to remove trapped moisture prior to use.  $\text{LiCoO}_2$  working electrodes were made using a typical slurry method by mixing  $\text{LiCoO}_2$ , super C65, and PI with a mass ratio of 90:5:5 in N-methyl-pyrrolidone solvent. PI was selected as the binder instead of PVDF, owing to the high thermal stability of PI. PVDF has a melting point of 177 °C, which is well below the ALD operation temperature of 225 °C. We found that PI-bound electrodes showed a slightly better cycling stability than PVDF-bound electrodes (Fig. S8 in the ESM). The average mass loading of active material ( $\text{LiCoO}_2$ ) was 15 mg·cm<sup>-2</sup>. For all ALD samples, they were calendared before ALD coating. For control samples, we also followed the same calendaring process on pristine  $\text{LiCoO}_2$  electrodes with exactly the same pressure applied.

$\text{LiAlO}_2$  was directly coated on  $\text{LiCoO}_2$  electrodes by using a Savannah S100 ALD system (Cambridge Nanotech).  $\text{LiAlO}_2$  ALD coating was developed based on previous literature reports [22]. Typical  $\text{LiAlO}_2$  ALD coating was prepared by alternating  $\text{Li}_2\text{O}$  and  $\text{Al}_2\text{O}_3$  sub-cycles under exposure mode to ensure high uniformity on high surface area substrates. The indicated number of ALD cycles in this article was counted by adding all  $\text{Li}_2\text{O}$  and  $\text{Al}_2\text{O}_3$  sub-cycles. For instance, a 20-cycle  $\text{LiAlO}_2$  ALD consisted of 10 super-cycles of one  $\text{Li}_2\text{O}$  sub-cycle and one  $\text{Al}_2\text{O}_3$  sub-cycle. The pulse, exposure, and purge sequence in a super cycle for lithium tert-butoxide, water, trimethylaluminum, and water was 2 s–20 s–30 s–0.015 s–20 s–30 s–0.015 s–20 s–30 s–0.015 s–20 s–30 s. For pure  $\text{Al}_2\text{O}_3$  ALD, the  $\text{Li}_2\text{O}$  sub-cycle was replaced by the  $\text{Al}_2\text{O}_3$  sub-cycle. All depositions were performed at 225 °C.

Lithium tert-butoxide was heated to 155–165 °C. Trimethylaluminum and water were kept at room temperature.

### 4.2 Electrochemical measurements

The battery cycling performance was evaluated by the galvanostatic cycling of coin cells (CR 2032) with Li foil (Alfa Aesar) as the counter electrode. The electrolyte consisted of 1.0 M  $\text{LiPF}_6$  in ethylene carbonate and diethyl carbonate with 1:1 volume ratio. Battery cycling data were collected using a LAND 8-channel battery tester with the potential window of 2.75–4.60 V vs.  $\text{Li}^+/\text{Li}$  at room temperature unless specified. The specific capacity was calculated based on the weight of  $\text{LiCoO}_2$ . After different numbers of cycles, coin cells were rested for 5 h prior to EIS measurements. EIS was conducted using a Biologic VSP potentiostat over the frequency range of 0.01 Hz to 1 MHz.

### 4.3 Material characterization

XRD (PANalytical X'Pert Diffractometer) was employed for phase identification, using  $\text{Cu K}\alpha$  radiation (0.15406 nm). TEM characterizations were conducted in a FEI Tecnai G2 F20 X-twin TEM system at an acceleration voltage of 200 kV. Raman spectroscopy was performed on a Horiba Labram HR Evolution Raman System with a 50 mW 532 nm excitation laser. XPS was performed on PHI 5000 VersaProbe, using an  $\text{Al K}\alpha$  ( $\lambda = 0.83$  nm;  $h\nu = 1,486.7$  eV) X-ray source operated at 2 kV and 20 mA. Elemental analysis was conducted using a Thermo Scientific XSERIES 2 ICP-MS system.

## Acknowledgements

Part of this work was performed at the Stanford Nano Shared Facilities (SNSF) and Stanford Nanofabrication Facility (SNF). We thank Allen Pei, Yongming Sun, and Kipil Lim for insightful discussion, Michelle Rincon, Christopher Neumann and Feifei Lian for technical assistance.

**Electronic Supplementary Material:** Supplementary material (experimental details and additional

characterizations) is available in the online version of this article at <https://doi.org/10.1007/s12274-017-1588-1>.

## References

- [1] Johnson, B. A.; White, R. E. Characterization of commercially available lithium-ion batteries. *J. Power Sources* **1998**, *70*, 48–54.
- [2] Winter, M.; Besenhard, J. O.; Spahr, M. E.; Novák, P. Insertion electrode materials for rechargeable lithium batteries. *Adv. Mater.* **1998**, *10*, 725–763.
- [3] Goodenough, J. B.; Kim, Y. Challenges for rechargeable Li batteries. *Chem. Mater.* **2010**, *22*, 587–603.
- [4] Etacheri, V.; Marom, R.; Elazari, R.; Salitra, G.; Aurbach, D. Challenges in the development of advanced Li-ion batteries: A review. *Energy Environ. Sci.* **2011**, *4*, 3243–3262.
- [5] Tarascon, J. M.; Armand, M. Issues and challenges facing rechargeable lithium batteries. *Nature* **2001**, *414*, 359–367.
- [6] Whittingham, M. S. Lithium batteries and cathode materials. *Chem. Rev.* **2004**, *104*, 4271–4301.
- [7] Cho, J.; Kim, Y. J.; Park, B. Novel LiCoO<sub>2</sub> cathode material with Al<sub>2</sub>O<sub>3</sub> coating for a Li ion cell. *Chem. Mater.* **2000**, *12*, 3788–3791.
- [8] Chen, Z. H.; Dahn, J. R. Studies of LiCoO<sub>2</sub> coated with metal oxides. *Electrochem. Solid-State Lett.* **2003**, *6*, A221–A224.
- [9] Chen, Z. H.; Dahn, J. R. Methods to obtain excellent capacity retention in LiCoO<sub>2</sub> cycled to 4.5 V. *Electrochim. Acta* **2004**, *49*, 1079–1090.
- [10] Jung, Y. S.; Cavanagh, A. S.; Dillon, A. C.; Groner, M. D.; George, S. M.; Lee, S. H. Enhanced stability of LiCoO<sub>2</sub> cathodes in lithium-ion batteries using surface modification by atomic layer deposition. *J. Electrochem. Soc.* **2010**, *157*, A75–A81.
- [11] Scott, I. D.; Jung, Y. S.; Cavanagh, A. S.; An, Y. F.; Dillon, A. C.; George, S. M.; Lee, S. H. Ultrathin coatings on nano-LiCoO<sub>2</sub> for Li-ion vehicular applications. *Nano Lett.* **2011**, *11*, 414–418.
- [12] Cho, J.; Kim, Y. J.; Kim, T. J.; Park, B. Zero-strain intercalation cathode for rechargeable Li-ion cell. *Angew. Chem., Int. Ed.* **2001**, *40*, 3367–3369.
- [13] Cho, J.; Kim, Y. J.; Park, B. LiCoO<sub>2</sub> cathode material that does not show a phase transition from hexagonal to monoclinic phase. *J. Electrochem. Soc.* **2001**, *148*, A1110–A1115.
- [14] Park, J. S.; Mane, A. U.; Elam, J. W.; Croy, J. R. Amorphous metal fluoride passivation coatings prepared by atomic layer deposition on LiCoO<sub>2</sub> for Li-ion batteries. *Chem. Mater.* **2015**, *27*, 1917–1920.
- [15] Jung, Y. S.; Lu, P.; Cavanagh, A. S.; Ban, C. M.; Kim, G. H.; Lee, S. H.; George, S. M.; Harris, S. J.; Dillon, A. C. Unexpected improved performance of ALD coated LiCoO<sub>2</sub>/graphite Li-ion batteries. *Adv. Energy Mater.* **2013**, *3*, 213–219.
- [16] Cao, H.; Xia, B. J.; Zhang, Y.; Xu, N. X. LiAlO<sub>2</sub>-coated LiCoO<sub>2</sub> as cathode material for lithium ion batteries. *Solid State Ionics* **2005**, *176*, 911–914.
- [17] Park, J. S.; Meng, X. B.; Elam, J. W.; Hao, S. Q.; Wolverton, C.; Kim, C.; Cabana, J. Ultrathin lithium-ion conducting coatings for increased interfacial stability in high voltage lithium-ion batteries. *Chem. Mater.* **2014**, *26*, 3128–3134.
- [18] Liu, J.; Banis, M. N.; Li, X. F.; Lushington, A.; Cai, M.; Li, R. Y.; Sham, T. K.; Sun, X. L. Atomic layer deposition of lithium tantalate solid-state electrolytes. *J. Phys. Chem. C* **2013**, *117*, 20260–20267.
- [19] Mäntymäki, M.; Hämäläinen, J.; Puukilainen, E.; Sajavaara, T.; Ritala, M.; Leskela, M. Atomic layer deposition of LiF thin films from Lithd, Mg(thd)<sub>2</sub>, and TiF<sub>4</sub> precursors. *Chem. Mater.* **2013**, *25*, 1656–1663.
- [20] Kozen, A. C.; Pearse, A. J.; Lin, C. F.; Noked, M.; Rubloff, G. W. Atomic layer deposition of the solid electrolyte LiPON. *Chem. Mater.* **2015**, *27*, 5324–5331.
- [21] Glass, A. M.; Nassau, K. Lithium ion conduction in rapidly quenched Li<sub>2</sub>O–Al<sub>2</sub>O<sub>3</sub>, Li<sub>2</sub>O–Ga<sub>2</sub>O<sub>3</sub>, and Li<sub>2</sub>O–Bi<sub>2</sub>O<sub>3</sub> glasses. *J. Appl. Phys.* **1980**, *51*, 3756–3761.
- [22] Aaltonen, T.; Nilsen, O.; Magrasó, A.; Fjellvåg, H. Atomic layer deposition of Li<sub>2</sub>O–Al<sub>2</sub>O<sub>3</sub> thin films. *Chem. Mater.* **2011**, *23*, 4669–4675.
- [23] Hu, Y.; Ruud, A.; Miikkulainen, V.; Norby, T.; Nilsen, O.; Fjellvåg, H. Electrical characterization of amorphous LiAlO<sub>2</sub> thin films deposited by atomic layer deposition. *RSC Adv.* **2016**, *6*, 60479–60486.
- [24] George, S. M. Atomic layer deposition: An overview. *Chem. Rev.* **2010**, *110*, 111–131.
- [25] Wang, H. F.; Jang, Y. I.; Huang, B. Y.; Sadoway, D. R.; Chiang, Y. M. TEM study of electrochemical cycling-induced damage and disorder in LiCoO<sub>2</sub> cathodes for rechargeable lithium batteries. *J. Electrochem. Soc.* **1999**, *146*, 473–480.
- [26] Levi, M. D.; Salitra, G.; Markovsky, B.; Teller, H.; Aurbach, D.; Heider, U.; Heider, L. Solid-state electrochemical kinetics of Li-ion intercalation into Li<sub>1-x</sub>CoO<sub>2</sub>: Simultaneous application of electroanalytical techniques SSCV, PITT, and EIS. *J. Electrochem. Soc.* **1999**, *146*, 1279–1289.
- [27] Ho, C.; Raistrick, I. D.; Huggins, R. A. Application of A-C techniques to the study of lithium diffusion in tungsten trioxide thin films. *J. Electrochem. Soc.* **1980**, *127*, 343–350.
- [28] Thomas, M. G. S. R.; Bruce, P. G.; Goodenough, J. B. AC impedance of the Li<sub>(1-x)</sub>CoO<sub>2</sub> electrode. *Solid State Ion.* **1986**, *18–19*, 794–798.
- [29] Thomas, M. G. S. R.; Bruce, P. G.; Goodenough, J. B. AC

- impedance analysis of polycrystalline insertion electrodes: Application to  $\text{Li}_{1-x}\text{CoO}_2$ . *J. Electrochem. Soc.* **1985**, *132*, 1521–1528.
- [30] Amatucci, G. G.; Tarascon, J. M.; Klein, L. C. Cobalt dissolution in  $\text{LiCoO}_2$ -based non-aqueous rechargeable batteries. *Solid State Ion.* **1996**, *83*, 167–173.
- [31] Baddour-Hadjean, R.; Pereira-Ramos, J. P. Raman microspectrometry applied to the study of electrode materials for lithium batteries. *Chem. Rev.* **2010**, *110*, 1278–1319.
- [32] Hadjiev, V. G.; Iliev, M. N.; Vergilov, I. V. The Raman spectra of  $\text{Co}_3\text{O}_4$ . *J. Phys. C: Solid State Phys.* **1988**, *21*, L199–L201.
- [33] Park, Y.; Kim, N. H.; Kim, J. M.; Kim, Y. C.; Jeong, Y. U.; Lee, S. M.; Choi, H. C.; Jung, Y. M. Surface reaction of  $\text{LiCoO}_2/\text{Li}$  system under high-voltage conditions by X-ray spectroscopy and two-dimensional correlation spectroscopy (2D-COS). *Appl. Spectrosc.* **2011**, *65*, 320–325.
- [34] Park, Y.; Kim, N. H.; Kim, J. Y.; Eom, I. Y.; Jeong, Y. U.; Kim, M. S.; Lee, S. M.; Choi, H. C.; Jung, Y. M. Surface characterization of the high voltage  $\text{LiCoO}_2/\text{Li}$  cell by X-ray photoelectron spectroscopy and 2D correlation analysis. *Vib. Spectrosc.* **2010**, *53*, 60–63.